Reducing the Peptidyl Features of Caspase-3 Inhibitors: A Structural Analysis

Joseph W. Becker,*,† Jennifer Rotonda,† Stephen M. Soisson,† Renee Aspiotis,‡ Christopher Bayly,‡ Sébastien Francoeur,‡,§ Michel Gallant,‡ Marga Garcia-Calvo,|| Andre Giroux,‡ Erich Grimm,‡ Yongxin Han,‡ Dan McKay,‡ Donald W. Nicholson,# Erin Peterson,|| Johanne Renaud,‡,⊥ Sophie Roy,# Nancy Thornberry,|| and Robert Zamboni‡

Departments of Medicinal Chemistry and Metabolic Disorders, Merck Research Laboratory, P.O. Box 2000, Rahway, New Jersey 07065, and Department of Medicinal Chemistry and Department of Biochemistry and Molecular Biology, Merck Frosst Center for Therapeutic Research, Merck-Frosst Canada & Co., P.O. Box 1005, Pointe Claire-Dorval, Quebec H9R 4P8, Canada

Received October 28, 2003

Caspases are cysteine proteases that specifically cleave Asp−Xxx bonds. They are key agents in inflammation and apoptosis and are attractive targets for therapy against inflammation, neurodegeneration, ischemia, and cancer. Many caspase structures are known, but most involve either peptide or protein inhibitors, unattractive candidates for drug development. We present seven crystal structures of inhibited caspase-3 that illustrate several approaches to reducing the peptidyl characteristics of the inhibitors while maintaining their potency and selectivity. The inhibitors reduce the peptidyl nature of inhibitors while preserving binding potency by (1) exploiting a hydrophobic binding site C-terminal to the cleavage site, (2) replacing the negatively charged aspartyl residue at P4 with neutral groups, and (3) using a peptidomimetic 5,6,7-tricyclic system or a pyrazinone at P2−P3. In addition, we have found that two nicotinic acid aldehydes induce a significant conformational change in the S2 and S3 subsites of caspase-3, revealing an unexpected binding mode. These results advance the search for caspase-directed drugs by revealing how unacceptable molecular features can be removed without loss of potency.

Introduction

The caspase family comprises a family of highly homologous cysteine proteases that play key roles in inflammation and apoptosis.[1−3] They display an unusual and strict specificity for cleavage after aspartyl residues. Caspases are expressed as inactive proenzymes of 30−50 kDa that include an amino-terminal domain of variable length and sequence that is followed by two domains of conserved sequences: a large subunit (approximately 20 kDa, designated p17 in caspase-3) and a small carboxy-terminal subunit (approximately 10 kDa, designated p12 in caspase-3). Activation is accomplished by proteolytic cleavage between these domains and subsequent assembly of heterotetramers that contain two copies each of the large and small subunits but lack the amino-terminal domains. Caspases can be divided into two main subfamilies by amino acid sequence homology, and this classification is reflected in the biological activities and substrate specificities of the members of these groups.[4] One family, exemplified by caspases-1, -4, and -5, is associated with inflammation, and the other, which contains caspases-3, -8, and -9, plays a key role in apoptosis. Within the second group, caspases act as either initiators or effectors of apoptosis: initiator caspases such as caspase-8 and -9 are activated by apoptotic stimuli and subsequently relocate within the cell to activate effector caspases such as caspase-3. Activator caspases cleave peptide bonds C-terminal to (V/I/L)EXD sequences, while effector caspases cleave after DEVD. Once activated, effector caspases carry out highly specific cleavage of target proteins associated with cellular homeostasis resulting in cell death. These processes are also affected by cofactors and inhibitors that modulate caspase activity, resulting in a highly regulated cascade of molecular events that control cell death in both normal development and disease.

Caspases are attractive targets for therapeutic intervention in several diseases because of the central role played by apoptosis in those conditions. Excessive, uncontrolled apoptosis appears to be related to several diseases that currently lack suitable treatment such as neurodegenerative disease, ischemia-reperfusion injury, and autoimmune disorders, suggesting that caspase inhibition may offer a significant opportunity for therapeutic intervention. In contrast, stimulation of caspase activity may represent a new path for approaching diseases such as cancer that are characterized by uncontrolled cell growth and that may be treated by regulating cell death.

Knowledge of an enzyme's specificity plays a key role in the design and development of specific inhibitors that can play a therapeutic role. Caspase substrate selectivity is regulated by recognition of the four amino acid sequence amino-terminal to the cleavage site.[4] Several three-dimensional structures of inhibited caspases have been determined, and the detailed information they

* To whom correspondence should be addressed. Phone: 732-594-3418. Fax: 732-594-5042. E-mail: joseph_becker@merck.com.
† Department of Medicinal Chemistry, Merck Research Laboratory.
‡ Department of Medicinal Chemistry, Merck-Frosst Canada & Co.
§ Present address: Département de Chimie, Université de Montréal, P.O. Box 6128, Station Downtown, Montréal H3C 3J7, Canada.
|| Department of Metabolic Disorders, Merck Research Laboratory.
Department of Biochemistry and Molecular Biology, Merck-Frosst Canada & Co.
⊥ Present address: Pharma Research, WKL-136.3.25, CH-4002 Basel, Switzerland.

10.1021/jm0305523 CCC: $27.50
Published on Web 04/06/2004

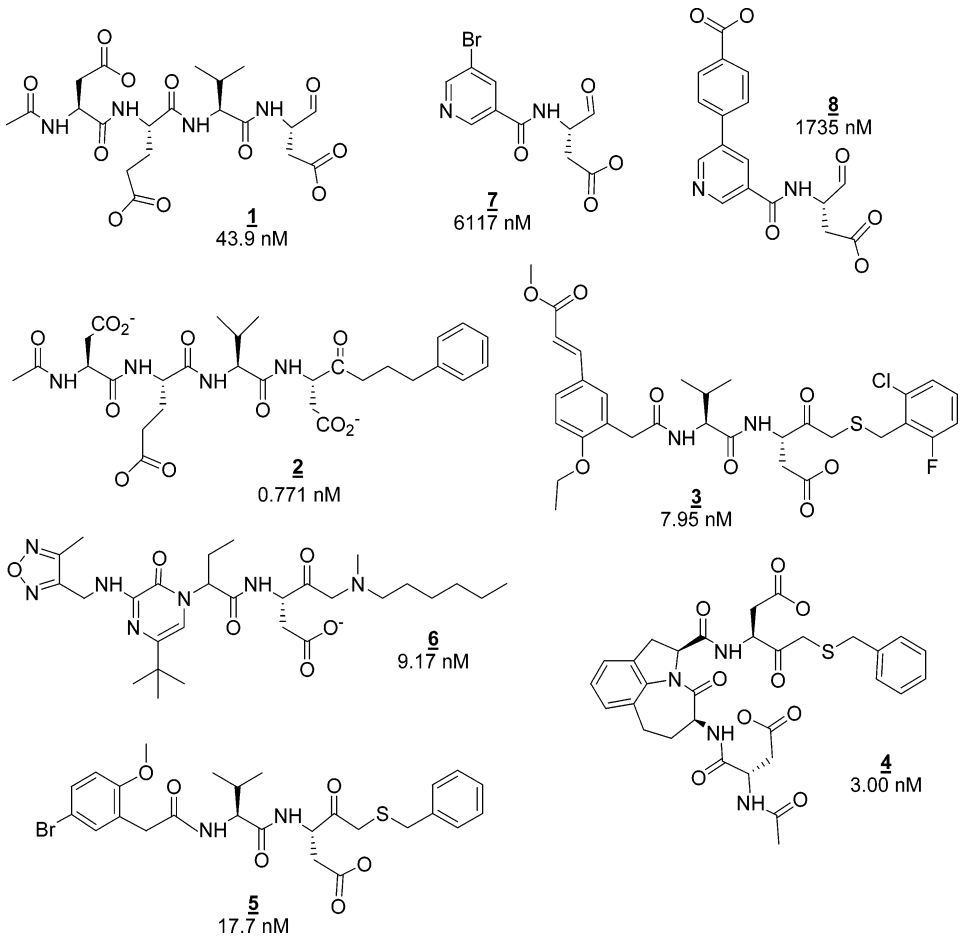

Figure 1. Caspase inhibitors used in this study. The structure, identifier, and IC_{50} in a caspase-3 inhibition assay[30] are shown.

have revealed is a guide to understanding the molecular features that affect the potency and selectivity of potential drugs. Available caspase structures involve complexes with both low molecular-weight ligands and macromolecular inhibitors, including studies on caspase-1,[5−11] caspase-3,[9,12−15] caspase-7,[9,15−17] caspase-8,[9,18−20] and caspase-9.[21] For caspase-7, structures of both the proenzyme[22,23] and the uninhibited mature enzyme[22] are also available.

The available structures of caspase/inhibitor complexes all involve peptide or protein inhibitors, with the single exception of a highly electrophilic isatin.[14] Peptides, however, are poor candidates for in vivo use as therapeutic agents because of poor metabolic stability and poor cell penetration. The initial caspase-3 inhibitor Ac-DEVD-aldehyde (**1**, Figure 1) has the additional liability of bearing three carboxylic acid groups and an aldehyde functionality, features that are expected to exacerbate these faults. Accordingly, one faces the task of removing the structural features that underlie these undesirable properties while preserving or enhancing the binding potency and selectivity of the peptide- or protein-based inhibitors. Here, we report structural studies on complexes between caspase-3 and inhibitors that were aimed at exploring a variety of approaches to solving this problem (Figure 1). These approaches center on three key areas of the binding site identified in previous work. First, we characterize interactions made C-terminal to the canonical tetrapeptide−aldehyde inhibitors when they are converted to ketones bearing alkyl−aromatic substituents that exploit a hydrophobic S1′ binding site [24] (compound **2**). Second, we report neutral replacements for the negatively charged P4 aspartyl residue, including a cinnamic acid methyl ester (**3**), a *p*-bromomethoxyphenyl group (**5**), and a furazan (**6**). We also describe two peptidomimetic groups that can be used to replace the P2−P3 dipeptide while preserving the bound conformation of the tetrapeptide leads as well as their essential polar interactions with the enzyme, a 5,6,7-tricyclic system (**4**) and a pyrazinone (**6**). In addition, we describe two nicotinic acid peptide replacements (**7**, **8**). We found, surprisingly, that these ligands produced significant conformational changes in the S2 and S3 subsites of the enzyme and make productive interactions with a previously unappreciated binding region.

Results and Discussion

Despite the variation in inhibitor and particularly in crystal lattice, the seven structures presented here are remarkably similar in tertiary and quaternary structure to one another and to the structure of the complex with **1**. When the eight independent p17/p12 homodimers are individually aligned with the complex with **1**, the rms deviation between α-carbon atoms ranges from 0.18 to 0.44 Å and the largest deviation is 1.70 Å. The largest deviations are at the ends of the loops near Lys175 and Phe381D. The strong conservation of the global protein fold is illustrated in Figure 2 (see also Table 1 in Supporting Information). Another global feature of these structures is the strong correlation of binding potency

Table 1. Crystallographic Parameters

	compound						
	2	**3**	**4**	**5**	**6**	**7**	**8**
space group	*I*222	$P2_12_12$	$P2_12_12$	*C*2	$P2_1$	*I*222	*C*2
unit cell params							
a (Å)	69.94	70.60	69.50	110.30	50.187	69.78	125.07
b (Å)	84.66	98.18	98.00	96.90	68.764	83.76	70.90
c (Å)	96.82	44.16	44.00	70.90	98.003	95.91	86.57
β (deg)				128.06	101.464		129.20
molecules/au	1	1	1	2	2	1	2
resoln (Å)	2.5	3.0	2.5	3.0	2.2	2.5	2.5
reflns	17 568	7630	29 312	15 975	101 766	19 330	42 258
unique rflns	8371	5527	9,500	11487	30,288	9319	18547
R_{merge} (%)	8.0	8.8	5.7	6.1	5.6	6.5	5.9
completeness (%)	81.6	84.1	88	96.8	95	92.9	89.5
R_{merge}	36.2	19.2	19.3	16.3	16.4	26.1	24.9
(highest shell) (%)	(2.59−2.50 Å)	(3.11−3.00 Å)	(2.60−2.50 Å)	(3.11−3.00 Å)	(2.28−2.20 Å)	(2.59−2.50 Å)	(2.59−2.50 Å)
completeness	33.3	75.0	25.0	88.7	76.6	48.2	33.3
(highest shell) (%)							
refinement software	XPLOR 3.1	X-PLOR 98.1	X-PLOR 98.1	X-PLOR 3.843	CNX 2000	XPLOR 3.1	XPLOR 3.1
R	0.1737	0.2256	0.1657	0.2787	0.2039	0.1845	0.1942
(highest shell)	0.2800	0.3370	0.2110	0.3490	0.2250	0.2680	0.3250
R_{free}	0.2304	0.3266	0.2123	0.3577	0.2515	0.2486	0.2470
(highest shell)	0.3380	0.3640	0.2420	0.4110	0.2850	0.3310	0.3900
rmsd bond (Å)	0.007	0.0095	0.007	0.009	0.006	0.006	0.007
rmsd angles (deg)	1.347	1.599	1.490	1.633	1.317	1.368	1.433
solvent molecules	77	34	100	24 (x2)	236	74	171
PDB code	1rhk	1rhr	1rhu	1rhq	1rhj	1re1	1rhm

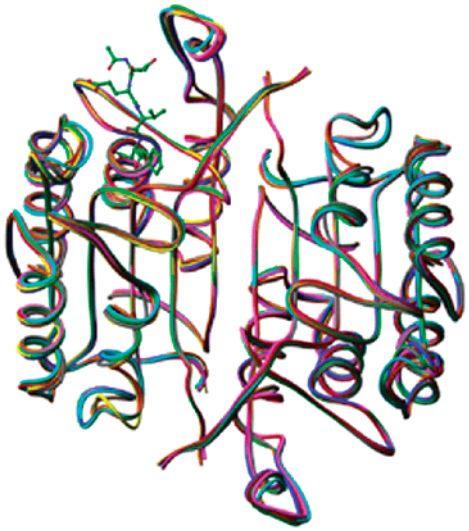

Figure 2. Schematic representation of the protein chains of the eight caspase-3 complexes presented in this work. The structures are aligned to the structure of the **1** complex, and the statistics of the alignment are given in Supporting Information Table 1. A model of **2** is shown in one molecule to indicate the active site of the enzyme.

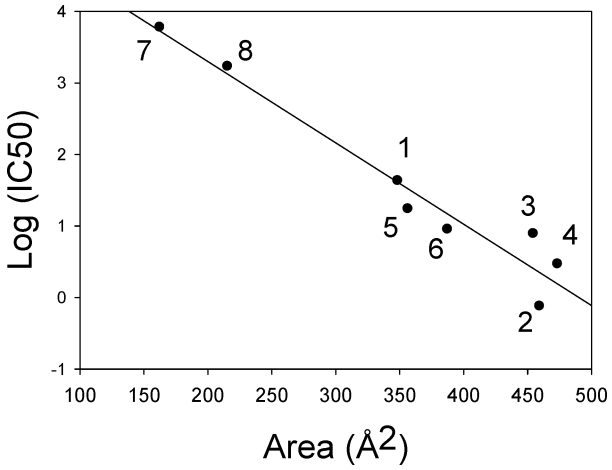

Figure 3. Plot of log(IC_{50}) vs area of caspase-3 solvent-accessible surface covered by bound inhibitor for the eight ligands listed in Figure 1. Excluded area was calculated with the AREAIMOL program of the CCP4 suite,[47] and linear regression ($r^2 = 0.95$) was used to fit the graph.

with the amount of solvent-accessible area covered by the bound ligands (Figure 3). The log(IC_{50}) is strongly linearly correlated ($r^2 = 0.95$) with excluded area over 4 orders of magnitude and the wide chemical diversity of the inhibitors studied.

S1′. In general, converting the P1 Asp-aldehyde in the initial peptide-based inhibitors to ketones and adding groups C-terminal to them afford an increase in binding energy. For example, conversion of the tetrapeptide−aldehyde inhibitor **1** to its phenylpropyl ketone **2** results in more than a 50-fold increase in binding potency (Figure 1). A less than 10-fold increase in potency of the methyl ketone (data not shown) suggests that while some of this increased binding energy is due to increased binding of the ketone moiety compared to the aldehyde, most of the improvement apparently arises from interactions with the S1′ binding site (Figure 4). This large, bowl-shaped, principally hydrophobic site is a C-terminal extension of the surface groove that contains S4−S1. It is delimited by the side chains of Met176, Thr177, Glu239, His237, Phe244, Cys285, Thr288, and Tyr338 and nearby peptide chains, and its shape offers little opportunity for highly specific interactions. Examination of S1′ suggested that, in terms of medicinal chemistry derivatization, considerable flexibility was allowed for substitution of medium-sized hydrophobic moieties at this site. The P1′ alkyl chain of **2** is in a generally extended configuration and covers an area of 107 Å^2. Conversion of the P1′ alkyl linker to a thioether, as in **3**−**5**, contributes additional binding energy: the all-carbon analogue of **5** binds caspase-3 15-fold more weakly than the thioether. The 2-Cl, 6-F aromatic substitution in **3** is apparently disordered; the density

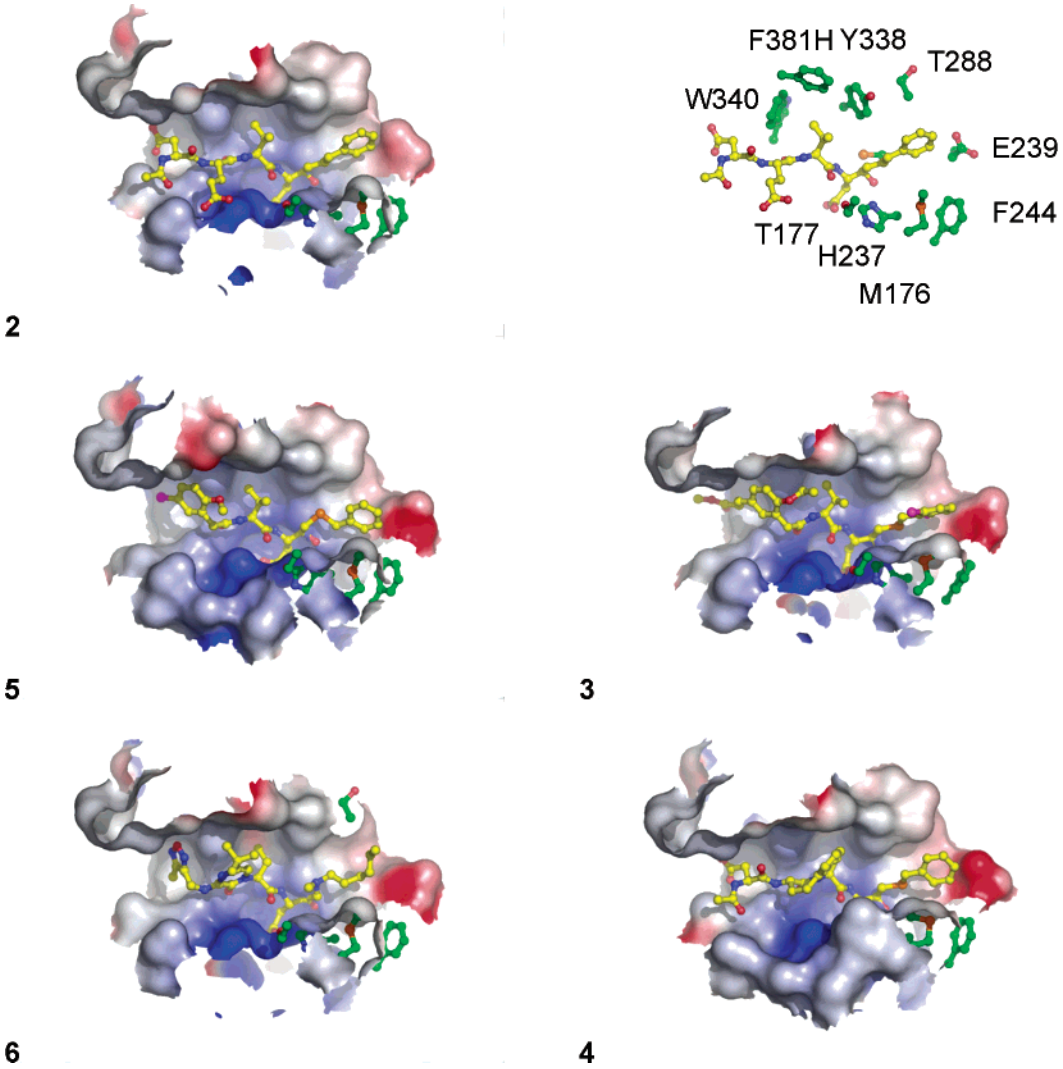

Figure 4. Interactions at S1′. For the five ligands with P1′ components, the inhibitor is shown in an electrostatic surface of the binding site. At the top right, **2** is shown surrounded by the side chains of residues in the S1′ subsite as well as the residues of the hydrophobic "wall" extending through S2 and S3. A stereo version of this figure is available in Supporting Information.

for this group is significantly weaker than that for the rest of the ligand (1.0σ−1.5σ vs 2.0σ), and parallel refinements failed to distinguish between a model with the fluorine pointing toward the carbonyl oxygen atoms of Gly238 and Gly287 and an alternative model with the chlorine in this position. There are no other polar contacts between caspase-3 and any atom of an inhibitor in S1′ indicating that the positive contributions to binding energy shown by these inhibitors arise from hydrophobic interactions. The relatively nonspecific nature of these interactions is reflected in the atomic mobility of the atoms in this subsite. For the two inhibitors with aromatic P1′ components whose individual temperature factors could be refined, the P1′ temperature factors are higher than those in P1−P4; the difference is 7.5 Å^2 in **2** and 12.9 Å^2 in **4**. In contrast with the alkyl aromatic moieties described above, the alkylamine at P1′ in **6** does not display a specific ordered conformation: there is no significant electron density for this chain despite the relatively high quality of the diffraction data and clear density and low temperature factors (approximately 25 Å^2) for the rest of this ligand. Consistent with these observations, the length of the alkyl chain does not contribute significantly to binding potency. For a series of compounds related to **6** with alkyl chains ranging from one to six carbon atoms, IC_{50} varies from 8 to 26 nM in a nonsystematic manner (data not shown).

S2−S3 Replacements. Studies employing positional-scanning peptide libraries demonstrated a strong preference for a glutamate side chain at P3,[4] but its polarity, along with that at P1 and P4, would interfere with the ability of potential drugs to penetrate their target cells. Analysis of the complex with **1** suggested that, of these three sites, P3 would be most likely to allow a neutral replacement without significant loss of potency. This side chain extends from the surface of the **1** and **2** complexes, making few hydrophobic contacts with the enzyme, and the carboxylate is highly exposed to solvent, suggesting that its contribution to binding might be low and that it could simply be removed. Stemming from this observation, conversion of the glutamyl residue of **2** to alanine resulted in only a roughly 2-fold decrease in IC_{50}. In addition, the removal of this polar group resulted in a roughly 3-fold increase in potency in a cell-based apoptosis assay (data not shown), consistent with improved permeability into cells. With this understanding of the S3 subsite, the

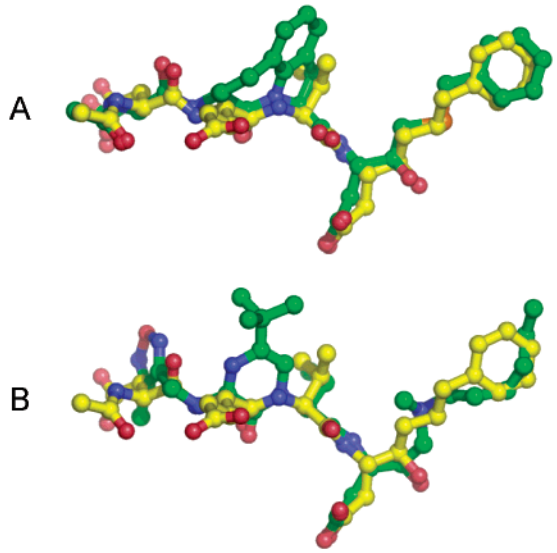

Figure 5. Peptide replacement at P2−P3. **2** (yellow carbon atoms) is superimposed on (A) **4** and (B) **6** (green carbon atoms). In each case, the structures were aligned using the α-carbon atoms of the enzyme, independent of the ligands.

medicinal chemistry effort left behind negatively charged P3 substituents.

In two ligands studied here, **4** and **6**, the P2−P3 peptide unit has been replaced with ring systems that reduce the peptide nature of the ligand but preserve significant binding potency (Figures 1 and 5), again with no carboxylate in P3. The 5,6,7-fused ring system in **4** has been proposed as a peptide replacement that would adopt a β-turn conformation,[25] but in this instance, the inhibitor displays the extended conformation shown by the peptide inhibitors **1** and **2**. To our knowledge, the present work is the first observation of this peptide replacement in a macromolecular complex. When the **2** and **4** complexes are aligned on the α-carbon atoms of the enzymes, the α-carbon atoms (or their topological equivalents) of the inhibitors show an rms deviation of only 0.49 Å (Figure 5A). In addition, the tricyclic system preserves atoms equivalent to those that make key peptide-specific hydrogen bonds between the ligand and the enzyme, the P2 N, the P3 N, and the P3 O (see Figure 4 of ref 12), so those hydrogen bonds are formed in both complexes. In addition, the tricyclic system makes extensive hydrophobic contacts with a hydrophobic "wall" comprising Tyr338, Trp340, and Phe381H and extending through S2−S3 (Figure 4).

Like **4**, **6** preserves the extended conformation of the peptide-based inhibitors (Figure 5B) as well as the three hydrogen bonds in P2 and P3, and it can be aligned closely with **2** (rmsd = 0.86 Å on α-carbon equivalents). **6** also makes significant hydrophobic contacts through S2 and S3: the substituted pyrazinone and the ethyl group at P2 make extensive contacts with the same hydrophobic wall as **4** (Figure 4).

The crystal structure of the **5** complex offered new insight into the medicinal chemistry effort by identifying a completely novel structural determinant for potency. The inhibitor makes the same interactions as peptide-based inhibitors **1** and **2** from S1 through to the S3 α-carbon but lacks the polar interactions made by the P3 glutamyl side chain, by the main chain P3 amide, and by the P4 aspartyl side chains (Figures 6A, 7A, and 7C). Instead, the bromoanisole moiety of **5** exhibits a previously unknown binding motif, making an extensive edge-to-face interaction with the side chain of Trp340 (Figures 4 and 7C). This contact lies on the opposite side of the active site cleft from S3, and we designate it as the "phenyl" site. The bromine atom of **5** protrudes into S4: in the aligned structures, it is 0.6 Å from the P4 carboxylate carbon of **1**. Clearly, replacing the bromine with short-chain elaborations into S4 with hydrogen-bond acceptors would improve potency. A number of successful replacements were found, of which **3** is an example.

S4 Replacements. The S4 subsite is a key determinant of binding selectivity among members of the caspase family,[4] and the differences in S4 binding specificities of caspases are reflected in the shape and chemical nature of this site in their three-dimensional structures.[5,6,9,12,18,19,22] One of the earliest insights offered to medicinal chemistry by the X-ray structure was the contrast between S1 and S4. While the positional scanning libraries showed equally strict preferences for a negatively charged aspartyl side chain in both sites,[4] the more open and uncharged structure of the S4 subsite suggested that it would be the more promising target for introduction of neutral alternatives to the aspartyl carboxylate. In contrast, the highly constricted and cationic S1 subsite presented a much more daunting challenge for replacement of the carboxylate. This analysis helped direct, and was consistent with, the subsequent medicinal chemistry optimization strategy directed at finding neutral replacements for carboxylic acid groups. The compounds studied here present three responses to this challenge that retain significant binding potency: the cinnamic acid methyl ester of **3** (7.95 nM), the *p*-bromomethoxyphenyl group of **5** (17.7 nM), and the furazan of **6** (9.17 nM). Ultimately the medicinal chemistry effort produced inhibitors retaining only one carboxylate, at P1.

3 binds similarly to **5**, with the anisole portion of the *p*-ethoxycinnamic acid methyl ester group lying in the phenyl site (Figures 4, 7C, and 7D). The ester group extends farther along the binding site than does the P4 carboxyl of **1**: when the complexes are aligned by their α-carbon atoms, the central carbon atom of the ester group of **3** is 1.66 Å from the carboxylate carbon of **1** (Figures 4, 7A, and 7D). Whereas the P4 aspartyl side chain hydrogen-bonds with the main chain amide proton of Phe381B and the $N^{\delta 2}$ of Asn342 (Figure 7A), the ester of **3** completely bypasses this interaction. Instead, the carbonyl oxygen atom of the ester forms a hydrogen bond with $N^{\epsilon 1}$ of Trp348 (Figure 7D).

In the **6** complex, the orientation of the P4 1,2,5-oxadiazole ring was unambiguously established by simulated-annealing-omit maps that clearly showed the position of the methyl group. This ring lies in the center of S4, but it does not make any of the contacts made by the acetyl or aspartyl groups of **1**. Its closest contacts are with the main chain amide nitrogen (3.20 Å) and carbonyl oxygen (2.94 Å) of Phe381B (Figure 7B). The angles among these atoms indicate that these interactions are not canonical hydrogen bonds. However, an ordered water molecule makes a bridged hydrogen-bond interaction between a furazan ring nitrogen atom and the side chain oxygen atom of Ser381C. Despite not

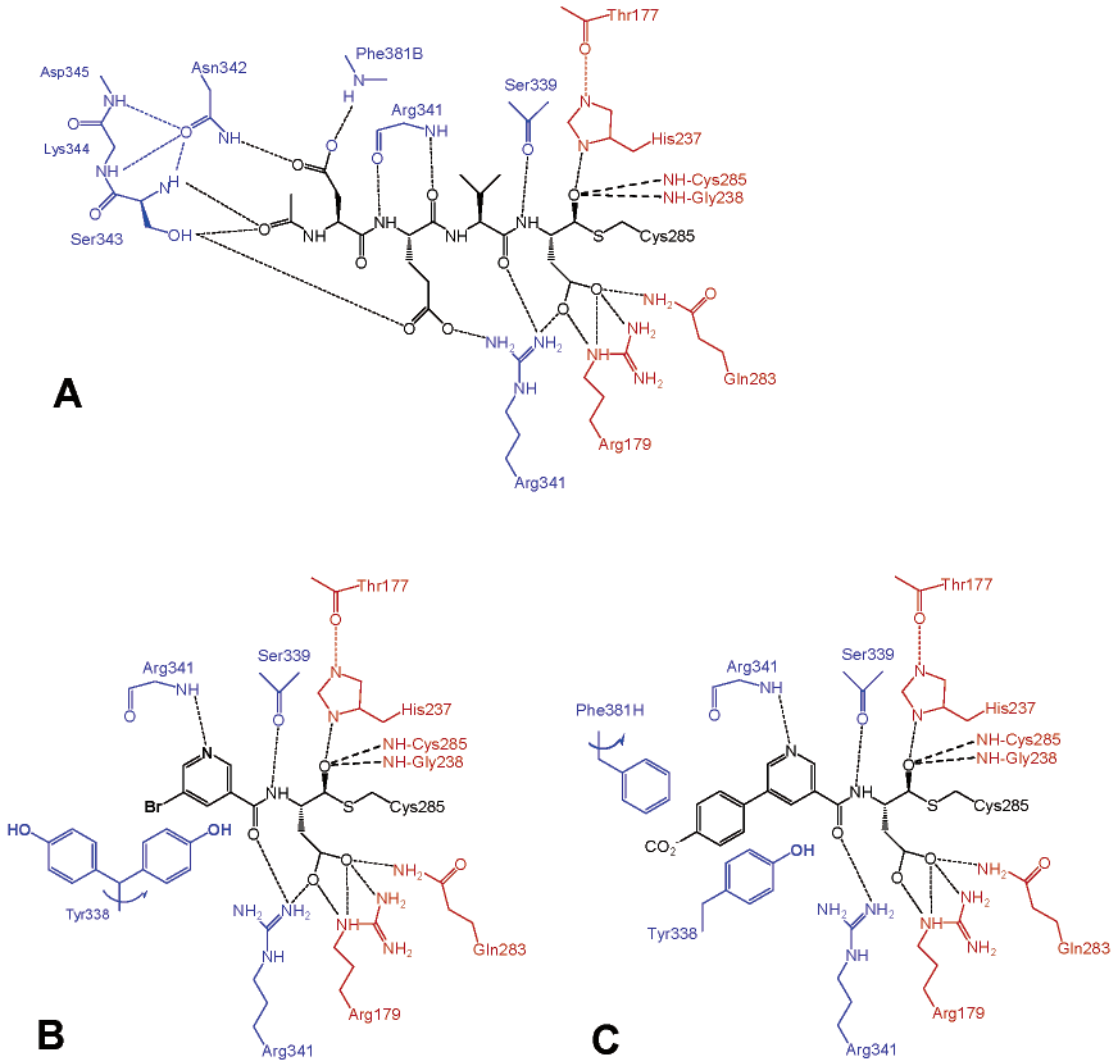

Figure 6. Interactions between caspase-3 and (A) **1**, (B) **7**, (C) **8**. The ligand-induced motions of Tyr338 (in part B) and Phe381H (in part C) are indicated. Protein residues from p17 are colored red, those from p12 are colored blue, and the inhibitors are colored black.

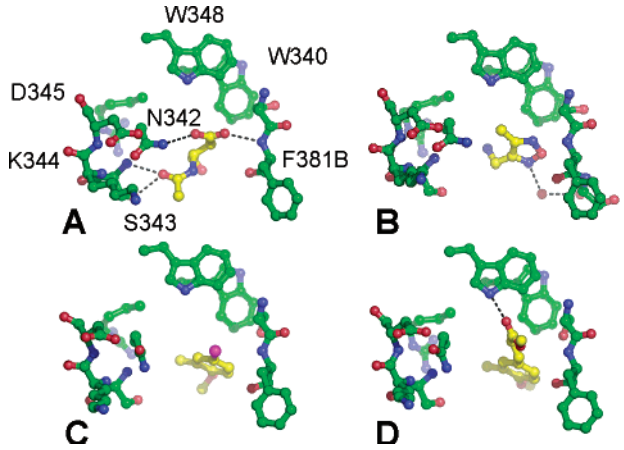

Figure 7. S4 subsites of caspase-3 complexes with (A) **1**, (B) **6**, (C) **5**, and (D) **3** in aligned protein structures. The P4 moiety is at the center of the inhibitor and is at the center of each figure. S4 residues are indicated in (A), and hydrogen bonds are depicted as dashed lines.

making the specific polar interactions of the P4 aspartyl group, the furazan makes significant contributions to binding strength. Its removal results in a 10-fold loss in IC_{50}, confirming that furazan is a potent neutral replacement for the anionic P4 aspartyl side chain of peptide-based inhibitors.

Nicotinic Acid Aldehydes. As part of a rapid-analogue synthesis effort to develop a more cell-penetrant series of inhibitors, compounds containing a P1 aspartyl aldehyde or ketone and a nicotinic acid derivative at P2−P3 were prepared.[26] Although these inhibitors (**7** and **8**, Figure 1) bound relatively weakly, their potency correlated well with their low molecular weights and the small area that they cover on the enzyme's surface (Figure 3). To optimize this lead, an attempt was made to model the binding of these compounds into the active site observed in the structure of the **1** complex. However, these calculations did not produce a satisfactory fit of the pyridyl ring into S2. The modeled position, over the part of the site that binds the P2−P3 amide carbonyl, passed in front of and effectively blocked S2 while making no good hydrophobic interactions, and this conformation did not explain the potency of this inhibitor compared to other close analogues. To understand the potency of **7** and **8** as a guide to lead optimization, we determined the crystal structures of the complexes with these two ligands.

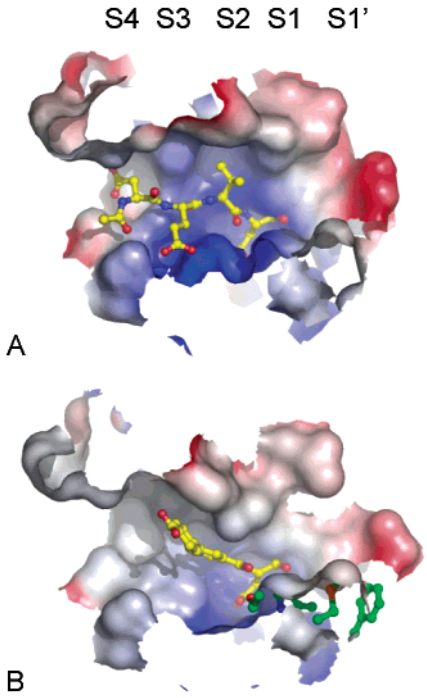

Figure 8. Binding site of caspase-3 represented as an electrostatic surface containing bound (A) **1** and (B) **8**. In the **8** complex, Tyr338 moves to occupy the volume filled by P2 Val in the **1** complex (top center of panel B), and Phe381H moves to make close contact with the *p*-carboxyphenyl ring of **8** (top left center of panel B). Compare with Figure 6 and the top right panel of Figure 4. A stereo version of this figure is available in Supporting Information.

As expected, the interactions in S1 are quite similar in the **1**, **7**, and two independent **8** complexes. The aspartic acid side chains at P1 make similar contacts in this positively charged site in all four structures, characterized by polar interactions with the side chains of Arg179, Gln283, and Arg341. In every case, interaction with the catalytic Cys285 results in a hemithioacetal, whose oxygen atoms point into the "oxyanion hole" of the catalytic site, making hydrogen bonds with the amide hydrogen atoms of Cys285 and Gly238 as well as with $N^{\delta 1}$ of the imidazole ring of the catalytic His237 (Figure 6).

The key to the potency of **7** and **8** lies in an unexpected and previously unobserved side chain movement. The side chain of Tyr338 rotates approximately 70° about X_1 in both nicotinic acid aldehyde complexes, from gauche+ to trans, into the volume occupied by the P2 Val side chain of the **1** inhibitor, essentially filling and thus obliterating S2 (Figures 6 and 8). The unsuccessful modeling calculations were based on the complex with **1** and had not predicted this side chain motion. The Tyr338 side chain interacts favorably with the pyridyl ring in both **7** and **8**. The inhibitors' pyridyl rings extend past S2 toward S3, with their nitrogens making excellent hydrogen bonds to the main chain amide of Arg341, analogous to the hydrogen bond between the P2−P3 amide carbonyl groups in the **1** complex. The X-ray structure of the **7** complex thus offered several insights to the medicinal chemistry effort. First, the binding of **7** in S2 was no longer an issue because this subsite no longer existed in the complex. Second, with the Tyr338 side chain movement, the interactions with the nicotinyl ring itself appeared optimal, and thus, additional potency would be sought only by elaborating the pyridyl ring toward S3 or S4. Third, the most direct access to S3 and S4 was via substitution para to the amide substituent, and this approach was used as a starting point for structure-based design.

The *p*-carboxyphenyl rings of **8** in both independent molecules do not lie in any of the previously identified subsites in caspase-3. Instead, the ring protrudes out of the binding site and makes relatively few contacts with the protein. The conformation of the *p*-carboxyphenyl ring differs in the two independent **8** complexes. In one molecule, the dihedral angle between the pyridyl and phenyl ring is approximately −40°, while in the second, it is +10°; consequently their binding interactions differ in the two molecules.

The primary contact is an aromatic interaction with the side chain of Phe381H, which moves from its position in the **1** and **7** complexes toward the bound **8** (Figures 6C and 8). This residue is in the nine-residue inserted loop that is present in caspase-3 but not in caspase-1. There are two independent molecules in the asymmetric unit of this crystal structure, and this loop moves toward the phenyl ring of **8** in both molecules, resulting in a net movement of 1.0−2.3 Å of the Phe381H side chain. In one of these molecules, the approximate distance between the phenyl ring and the phenylalanine side chain is 4.0 Å. In the second molecule, the distance is approximately 4.6 Å, resulting in productive interactions with the phenyl ring of **8**, and this contact probably accounts for most of the increased binding strength of **8**. The first molecule has one of the carboxyl oxygens hydrogen-bonded to the terminal nitrogen (N^{ζ}) of the side chain of Lys175 of a symmetry-related second protein molecule. The second inhibitor molecule has one of the carboxyl oxygens making an intramolecular hydrogen bond to the side chain oxygen (O^{γ}) of Ser331C. The other carboxyl oxygen is hydrogen-bonded to the side chain oxygen (O^{γ}) of Ser175A of the symmetry-related first protein molecule.

The unexpected binding mode and ligand-induced conformational changes in the nicotinic acid aldehyde complexes make clear the importance of obtaining structures representative of any new ligand class. They also revealed a previously unsuspected region of caspase-3 near Phe381H that can make productive binding interactions that do not require peptide-like structural elements. The location and nature of this site also raise the possibility of designing inhibitors that are branched off the nicotinyl ring in order to exploit the opportunities for binding potency offered by the new site as well as the previously known S4.

In the work presented here, we report the structural details of multiple approaches to removing undesirable formal charges and peptide bonds from initial, substrate-based inhibitors of caspase-3. Converting charged peptide leads such as those arising from early caspase research to therapeutically acceptable agents requires the simultaneous solution of multiple problems: the peptide bonds and charges must be removed while potency is maintained or increased. At the same time, appropriate absorption, metabolic, distribution, and excretion properties must be obtained. To meet these multiple goals, it is important to investigate multiple pathways of ligand modification and to understand the

structural, chemical, and pharmaceutical properties of these modifications. Our work has revealed the structural details of modifications that improve the properties of the initial peptide leads at several sites. We show the details of how alkyl−aromatic substituents at P1′ can add binding potency to caspase inhibitors by interacting with a shallow hydrophobic S1′ subsite but that purely alkyl substituents at this location do not enhance binding. Even though a negatively charged aspartyl group is strictly required at P4 in peptide-based inhibitors, our results reveal how uncharged groups including a cinnamic acid methyl ester, a *p*-bromomethoxyphenyl group, and a furazan can form productive interactions with the S4 subsite of caspase-3. We also show the structural basis for the successful reduction of the peptidyl character at P2−P3 through use of a 5,6,7-fused ring system or a pyrazinone. A previously unobserved phenyl binding site provides an alternative route to S4 without using S3 at all, an approach that proved particularly useful because S3 offered little potential for increasing potency. Both of these peptide replacements preserve the extended conformation of the original peptide inhibitor as well as the crucial protein−ligand hydrogen bonds, and they provide productive van der Waals interactions with a hydrophobic surface that defines the substrate-binding groove of caspase-3. To our knowledge, the present work represents the first detailed structural analysis of the tricyclic ring system or a pyrazinone as part of a macromolecular ligand, as well as of the use of non-aspartyl groups in S4 of an effector caspase. Finally, our work has revealed an unexpected mobility in the S2 subsite of caspase-3. We found that the potency of two nicotinic acid aldehydes could only be understood by accounting for the induced conformational changes in this region of the enzyme and the ensuing changes to the protein−ligand interactions.

Experimental Section

Caspase-3 was prepared by refolding active enzyme from its constituent p17 and p12 subunits, followed by affinity purification with the ligand of interest and/or ion exchange chromatography as described.[12,27] Expression and purification of His-tagged caspase-3 was performed essentially as described in Xanthoudakis et al.[28] Briefly, the coding region of procaspase-3 flanked by NdeI and XhoI restriction sites at the N- and C-termini, respectively, was subcloned in the NdeI and XhoI sites of the prokaryotic expression vector pET20b+, placing the procaspase-3 coding region in frame with a His tag at the C-terminus. After transformation into the protease-deficient strain of *Escherichia coli*, BL21 (DE3) (Novagen), a single colony was used to inoculate M9 medium containing 100 μg/mL carbenicillin. The culture was first incubated at 37 °C until it reached an OD_{600} of 0.6−0.8, after which the culture was cooled to 27 °C and protein expression was induced with 1 mM isopropyl β-D-thiogalactoside for 90 min. Bacterial pellets were harvested by centrifugation and stored at −80 °C. All the purification steps were carried out at 4 °C. The cell pellets were thawed in buffer A (20 mM Tris·HCl, pH 8.0, 20 mM imidazole, 2.5 mM β-mercaptoethanol) containing 1% Triton X-100 and lysed by sonication. The extract was clarified by centrifugation at 10000*g* for 30 min, and the supernatant solution was filtered through 0.22 μm syringe driven filters (Millipore) and loaded onto a column (bed volume = 1 mL of gel per liter of cell culture) of Ni-NTA agarose (Qiagen) equilibrated in buffer A. The column was extensively washed with this buffer, and the protein was eluted from the resin using a linear gradient from 20 to 250 mM imidazole in buffer A. Fractions were collected and analyzed for purity by SDS−PAGE on 10% Tricine gels (Invitrogen) and for protein concentration using BSA as a standard.[29] Caspase-3 activity was monitored in a fluorometric assay as described,[30] with DEVD·AMC as a substrate. Fractions showing the highest purity and activity were pooled, dialyzed against 100 mM HEPES·NaOH, 10% sucrose, 0.1% CHAPS, 10 mM DTT, pH 7.5, and used for crystallographic studies. The overall yield of active caspase-3 was 2−6 mg of purified protein per liter of culture.

Caspase-3/ligand complexes were crystallized by hanging-drop vapor diffusion using the conditions described in Supporting Information Table 2. In each case, equal volumes of protein and well solutions were mixed to initiate crystallization. Although the crystallization conditions were quite similar for each complex, the seven complexes produced five different crystal forms (Table 1). With one exception, diffraction data were collected at room temperature using a Siemens multiwire area detector and Cu Kα radiation produced by a Rigaku RU-200 rotating-anode X-ray generator. These data were processed with the SAINT software package,[31] and the statistics of data collection and reduction are listed in Table 1. Data from the **6** complex were collected at beamline 17-ID at the facilities of the Industrial Macromolecular Crystallographic Association Collaborative Access Team at the Advanced Photon Source (Argonne National Laboratory, Argonne, IL) using a Mar CCD detector. For this experiment, a crystal was soaked in 25% glycerol and vitrified in a vapor stream from a liquid nitrogen source. These data were processed with HKL2000.[32] All structures were solved by molecular replacement, using the protein portion of the caspase-3/**1** structure[12] as probe. Models of the bound ligands were constructed in QUANTA[33] and refined using CHARMM.[34] Refinement restraints based on the resulting models were generated in XPLO2D.[35] As listed in Table 1, X-PLOR[36] and CNX[37] were used for the molecular replacement and refinement calculations. During the refinement of each complex, at least one round of simulated annealing refinement was performed to remove model bias,[38] and a final round of refinement was performed using CNX. Low-resolution and weak-intensity rejection criteria were not applied in refinement and map calculation. For cross-validation,[39] 10% of the data were set aside and never used in any refinement. Individual atomic temperature factors were refined in all refinements with the exception of the **3** and **5** complexes where only two temperature factors per residue, one for main chain and one for side chain atoms, were employed. Strict noncrystallographic symmetry constraints were applied in the refinement of the **5** complex, and these constraints played a crucial role in the interpretation of this relatively low-resolution structure. The current models were built by interactive model building using CHAIN[40] and O,[41,42] adding water molecules based on peak heights in difference electron density maps and appropriate contacts with hydrogen-bonding partners. Each model contains p17 (residues 150−295) and p12 (residues 320−401) chains, bound inhibitor, and solvent. In each structure, the inhibitor forms a hemithioacetal or hemithioketal with the active-site cysteine residue. Final refinement statistics are listed in Table 1. Coordinates and structure factors have been deposited in the Protein Data Bank[43] (access codes 1re1, 1rhj, 1rhk, 1rhm, 1rhq, 1rhr, 1rhu) for release upon publication. Figure 2 was prepared with RIBBONS,[44] and Figures 4, 5, 7, and 8 were prepared with PyMOL.[45] The electrostatic surfaces in Figures 4 and 8 were calculated with GRASP.[46]

Acknowledgment. Diffraction data were collected at beamline 17-ID in the facilities of the Industrial Macromolecular Crystallography Association Collaborative Access Team (IMCA-CAT) at the Advanced Photon Source. These facilities are supported by the companies of the Industrial Macromolecular Crystallography Association through a contract with Illinois Institute of Technology (IIT), executed through IIT's Center for Synchrotron Radiation Research and Instrumentation.

Supporting Information Available: Statistical comparison of the alignment of the structures presented here, detailed crystallization conditions, and stereo versions of Figures 4, 7, and 8. This material is available free of charge via the Internet at http://pubs.acs.org.

References

(1) Thornberry, N. A.; Lazebnik, Y. Caspases: Enemies Within. *Science* **1998**, *281*, 1312−1316.

(2) Nicholson, D. W. Caspase Structure, Proteolytic Substrates, and Function during Apoptotic Cell Death. *Cell Death Differ.* **1999**, *6*, 1028−1042.

(3) Stennicke, H. R.; Ryan, C. A.; Salvesen, G. S. Reprieval from Execution: The Molecular Basis of Caspase Inhibition. *Trends Biochem. Sci.* **2002**, *27*, 94−101.

(4) Thornberry, N. A.; Rano, T. A.; Peterson, E. P.; Rasper, D. M.; Timkey, T.; et al. A Combinatorial Approach Defines Specificities of Members of the Caspase Family and Granzyme-B−Functional, Relationships Established for Key Mediators Of Apoptosis. *J. Biol. Chem.* **1997**, *272*, 17907−17911.

(5) Wilson, K. P.; Black, J.; Thomson, J. A.; Kim, E. E.; Griffith, J. P.; et al. Structure and Mechanism of Interleukin-1-beta Converting-Enzyme. *Nature* **1994**, *370*, 270−275.

(6) Walker, N. P. C.; Talanian, R. V.; Brady, K. D.; Dang, L. C.; Bump, N. J.; et al. Crystal-Structure of the Cysteine Protease Interleukin-1-Beta-Converting Enzyme−A (P20/P10)(2) Homodimer. *Cell* **1994**, *78*, 343−352.

(7) Rano, T. A.; Timkey, T.; Peterson, E. P.; Rotonda, J.; Nicholson, D. W.; et al. A Combinatorial Approach for Determining Protease Specificities: Application to Interleukin-1beta Converting Enzyme (ICE). *Chem. Biol.* **1997**, *4*, 149−155.

(8) Okamoto, Y.; Anan, H.; Nakai, E.; Morihira, K.; Yonetoku, Y.; et al. Peptide Based Interleukin-1 Beta Converting Enzyme (ICE) Inhibitors: Synthesis, Structure Activity Relationships and Crystallographic Study of the ICE−Inhibitor Complex. *Chem. Pharm. Bull.* **1999**, *47*, 11−21.

(9) Wei, Y.; Fox, T.; Chambers, S. P.; Sintchak, J.; Coll, J. T.; et al. The Structures of Caspases-1, -3, -7, and -8 Reveal the Basis for Substrate and Inhibitor Selectivity. *Chem. Biol.* **2000**, *7*, 432−441.

(10) Shahripour, A. B.; Plummer, M. S.; Lunney, E. A.; Sawyer, T. K.; Stankovic, C. J.; et al. Structure-Based Design of Caspase-1 Inhibitor Containing a Diphenyl Ether Sulfonamide. *Bioorg. Med. Chem. Lett.* **2001**, *11*, 2779−2782.

(11) Shahripour, A. B.; Plummer, M. S.; Lunney, E. A.; Albrecht, H. P.; Hays, S. J.; et al. Structure-Based Design of Nonpeptide Inhibitors of Interleukin-1 Beta Converting Enzyme (ICE, Caspase-1). *Bioorg. Med. Chem.* **2002**, *10*, 31−40.

(12) Rotonda, J.; Nicholson, D. W.; Fazil, K. M.; Gallant, M.; Gareau, Y.; et al. The 3-Dimensional Structure of Apopain/Cpp32, a Key Mediator of Apoptosis. *Nat. Struct. Biol.* **1996**, *3*, 619−625.

(13) Mittl, P. R. E.; Dimarco, S.; Krebs, J. F.; Bai, X.; Karanewsky, D. S.; et al. Structure of Recombinant Human Cpp32 in Complex with the Tetrapeptide Acetyl-Asp-Val-Ala-Asp Fluoromethyl Ketone. *J. Biol. Chem.* **1997**, *272*, 6539−6547.

(14) Lee, D.; Long, S. A.; Adams, J. L.; Chan, G.; Vaidya, K. S.; et al. Potent and Selective Nonpeptide Inhibitors of Caspases 3 and 7 Inhibit Apoptosis and Maintain Cell Functionality. *J. Biol. Chem.* **2000**, *275*, 16007−16014.

(15) Riedl, S. J.; Renatus, M.; Schwarzenbacher, R.; Zhou, Q.; Sun, C. H.; et al. Structural Basis for the Inhibition of Caspase-3 by XIAP. *Cell* **2001**, *104*, 791−800.

(16) Huang, Y. H.; Park, Y. C.; Rich, R. L.; Segal, D.; Myszka, D. G.; et al. Structural Basis of Caspase Inhibition by XIAP: Differential Roles of the Linker versus the BIR Domain. *Cell* **2001**, *104*, 781−790.

(17) Chai, J. J.; Shiozaki, E.; Srinivasula, S. M.; Wu, Q.; Dataa, P.; et al. Structural Basis of Caspase-7 Inhibition by XIAP. *Cell* **2001**, *104*, 769−780.

(18) Blanchard, H.; Kodandapani, L.; Mittl, P. R. E.; Di Marco, S.; Krebs, J. F.; et al. The Three-Dimensional Structure of Caspase-8: An Initiator Enzyme in Apoptosis. *Struct. Folding Des.* **1999**, *7*, 1125−1133.

(19) Watt, W.; Koeplinger, K. A.; Mildner, A. M.; Heinrikson, R. L.; Tomasselli, A. G.; et al. The Atomic-Resolution Structure of Human Caspase-8, a Key Activator of Apoptosis. *Struct. Folding Des.* **1999**, *7*, 1135−1143.

(20) Xu, G. Z.; Cirilli, M.; Huang, Y. H.; Rich, R. L.; Myszka, D. G.; et al. Covalent Inhibition Revealed by the Crystal Structure of the Caspase-8/P35 Complex. *Nature* **2001**, *410*, 494−497.

(21) Renatus, M.; Stennicke, H. R.; Scott, F. L.; Liddington, R. C.; Salvesen, G. S. Dimer Formation Drives the Activation of the Cell Death Protease Caspase 9. *Proc. Natl. Acad. Sci. U.S.A.* **2001**, *98*, 14250−14255.

(22) Chai, J.; Wu, Q.; Shiozaki, E.; Srinivasula, S. M.; Alnemri, E. S.; et al. Crystal Structure of a Procaspase-7 Zymogen. Mechanisms of Activation and Substrate Binding. *Cell* **2001**, *107*, 399−407.

(23) Riedl, S. J.; Fuentes Prior, P.; Renatus, M.; Kairies, N.; Krapp, S.; et al. Structural Basis for the Activation of Human Procaspase-7. *Proc. Natl. Acad. Sci. U.S.A.* **2001**, *98*, 14790−14795.

(24) Schechter, I.; Berger, A. On the size of the active site in proteases. I. Papain. *Biochem. Biophys. Res. Commun.* **1967**, *27*, 157−162.

(25) Hanessian, S.; McNaughton-Smith, G.; Lombart, H.-G.; Lubell, W. D. Design and Synthesis of Conformationally Constrained Amino Acids as Versatile Scaffolds and Peptide Mimetics. *Tetrahedron* **1997**, *53*, 12789−12854.

(26) Isabel, E.; Black, W. C.; Bayly, C. I.; Grimm, E. L.; Janes, M. K.; et al. Nicotinyl Aspartyl Ketones as Inhibitors of Caspase-3. *Bioorg. Med. Chem. Lett.* **2003**, *13*, 2137−2140.

(27) Garcia-Calvo, M.; Peterson, E. P.; Rasper, D. M.; Vaillancourt, J. P.; Zamboni, R.; et al. Purification and Catalytic Properties of Human Caspase Family Members. *Cell Death Differ.* **1999**, *6*, 362−369.

(28) Xanthoudakis, S.; Roy, S.; Rasper, D.; Hennessey, T.; Aubin, Y.; et al. HSP60 Accelerates the Maturation of Pro-Caspase-3 by Upstream Activator Proteases During Apoptosis. *EMBO J.* **1999**, *18*, 2049−2056.

(29) Bradford, M. M. A Rapid and Sensitive Method for the Quantitation of Microgram Quantities of Protein Utilizing the Principle of Protein−Dye Binding. *Anal. Biochem.* **1976**, *72*, 248.

(30) Nicholson, D. W.; Ali, A.; Thornberry, N. A.; Vaillancourt, J. P.; Ding, C. K.; et al. Identification and Inhibition of the Ice/Ced-3 Protease Necessary for Mammalian Apoptosis. *Nature* **1995**, *376*, 37−43.

(31) *SAINT Software Reference Manual*; Siemens Analytical Instruments: Madison, WI, 1995.

(32) Otwinowski, Z.; Minor, W. Processing of X-ray Diffraction Data Collected in Oscillation Mode. *Methods in Enzymology*; Academic Press: San Diego, CA, 1997; Vol. 276, pp 307−326.

(33) *QUANTA*; Accelrys: San Diego, CA, 1984.

(34) Brooks, B.; Bruccoleri, R.; Olafson, B.; States, D.; Swaminathan, S.; et al. CHARMM: A Program for Macromolecular Energy, Minimization, and Molecular Dynamics Calculations. *J. Comput. Chem.* **1983**, *4*, 187−217.

(35) Kleywegt, G. J.; Zou, J.-Y.; Kjeldgaard, M.; Jones, T. A. Around O. In *International Tables for Crystallography, Vol. F, Crystallography of Biological Macromolecules*; Kluwer Academic Publishers: Dordrecht, The Netherlands, 2001, pp 353−356.

(36) Brünger, A. T. *X-PLOR: Version 3.1, a System for X-Ray Crystallography and NMR*; Yale University Press: New Haven, CT, 1992.

(37) Brünger, A. T.; Adams, P. D.; Clore, G. M.; DeLano, W. L.; Gros, P.; et al. Crystallography & NMR System: A New Software Suite for Macromolecular Structure Determination. *Acta Crystallogr.* **1998**, *D54*, 905−921.

(38) Hodel, A.; Kim, S.-H.; Brünger, A. T. Model Bias in Macromolecular Crystal Structures. *Acta Crystallogr.* **1992**, *A48*, 851−858.

(39) Brünger, A. T. Free *R* Value: A Novel Statistical Quantity for Assessing the Accuracy of Crystal Structures. *Nature* **1992**, *355*, 472−475.

(40) Sack, J. S. CHAIN−A Crystallographic Modeling Program. *J. Mol. Graphics* **1988**, *6*, 224−225.

(41) Jones, T. A.; Zou, J. Y.; Cowan, S. W.; Kjeldgaard, M. Improved Methods for Binding Protein Models in Electron Density Maps and the Location of Errors in These Models. *Acta Crystallogr A* **1991**, *A47*, 110−119.

(42) Jones, T. A.; Kjeldgaard, M. Electron-Density Map Interpretation. *Methods Enzymol.* **1997**, *277*, 173−208.

(43) Berman, H. M.; Westbrook, J.; Feng, Z.; Gilliland, G.; Bhat, T. N.; et al. The Protein Data Bank. *Nucleic Acids Res.* **2000**, *28*, 235−242.

(44) Carson, M. Ribbons. *Methods in Enzymology*; Academic Press: New York, 1997; pp 493−505.

(45) DeLano, W. L. *The PyMOL Molecular Graphics System*; DeLano Scientific: San Carlos, CA, 2002.

(46) Nicholls, A.; Sharp, K. A.; Honig, B. Protein folding and association: insights from the interfacial and thermodynamic properties of hydrocarbons. *Proteins* **1991**, *11*, 281−296.

(47) Bailey, S. The CCP4 Suite−Programs for Protein Crystallography. *Acta Crystallogr.* **1994**, *D50*, 760−763.

JM0305523